Supplemental material: "Evolution of the Normal State of a Strongly Interacting Fermi Gas from a Pseudogap Phase to a Molecular Bose Gas"

A. Perali [1], F. Palestini [1], P. Pieri [1], G. C. Strinati[1], J. T. Stewart [2], J. P. Gaebler [2], T. E. Drake [2], D. S. Jin[2]
[1] *Dipartimento di Fisica, Università di Camerino, I-62032 Camerino, Italy*
[2] *JILA, Quantum Physics Division, NIST and Department of Physics, University of Colorado, Boulder, CO 80309-0440, USA*

We provide details of the theoretical calculations of the wave-vector resolved rf signal and a description of the experimental procedures. We also add information about the theoretical analysis of the experimental data.

PACS numbers: 03.75.Ss,03.75.Hh,74.40.-n,74.20.-z

Pairing-fluctuation theory

The theoretical approach of Ref. [1] is based on a diagrammatic t-matrix approximation, whereby the fermionic single-particle self-energy $\Sigma(\mathbf{k},\omega)$ includes pairing fluctuations. We have used that approach here to calculate the single-particle spectral function $A(\mathbf{k},\omega)$ for the homogeneous case:

$$A(\mathbf{k},\omega) = -\frac{1}{\pi}\frac{\mathrm{Im}\Sigma(\mathbf{k},\omega)}{[\omega-\xi_{\mathbf{k}}-\mathrm{Re}\Sigma(\mathbf{k},\omega)]^2+[\mathrm{Im}\Sigma(\mathbf{k},\omega)]^2} \quad (1)$$

where $\xi_{\mathbf{k}} = \mathbf{k}^2/(2m)-\mu$. For given wave vector $\mathbf{k}$, the frequency structure of the real and imaginary parts of $\Sigma(\mathbf{k},\omega)$ determines the positions and widths of the peaks in $A(\mathbf{k},\omega)$, and is thus responsible for the nontrivial shape of the dispersions of these peaks vs $k=|\mathbf{k}|$.

Wave-vector resolved rf spectroscopy

When final-state effects in the rf transition [2, 3] can be neglected (like for the case of ^{40}K used in the experiment), the rf signal in the normal phase is given by [3]:

$$\mathrm{RF}(\tilde{\omega}) = \frac{1}{\pi N}\int d\mathbf{r}\int\frac{d\mathbf{k}}{(2\pi)^3}A(\mathbf{k},\xi(\mathbf{k};\mathbf{r})-\tilde{\omega})f(\xi(\mathbf{k};\mathbf{r})-\tilde{\omega}). \quad (2)$$

Here, $\tilde{\omega}=\omega_{\mathrm{rf}}-\omega_a$ is the detuning frequency where ω_{rf} is the frequency of the rf photon and ω_a the atomic hyperfine frequency, $\mathbf{r}$ the position in the trap, $\xi(\mathbf{k};\mathbf{r}) = \mathbf{k}^2/(2m)-\mu+V(\mathbf{r})$ a local energy with trapping potential $V(\mathbf{r}) = m\left(\omega_x x^2+\omega_y y^2+\omega_z z^2\right)/2$, and $f(\epsilon) = \left(e^{\epsilon/(k_BT)}+1\right)^{-1}$ the Fermi function. [The prefactor in Eq.(2) is chosen to make the total area of the rf signal equal unity.] Equation (2) is based on a local-density approximation where contributions of adjacent shells in the trap are separately considered.

The rf signal can be analyzed into its individual $\mathbf{k}$-components to compare with the experimental technique of Ref. [4]. The resulting *wave-vector resolved rf signal* is obtained by dropping the $\mathbf{k}$-integration and considering one $\mathbf{k}$-component at a time. More precisely, the selection is made over the magnitude $k=|\mathbf{k}|$ while $\hat{k}=\mathbf{k}/k$ is integrated over the solid angle, yielding:

$$\mathrm{RF}(k,\tilde{\omega}) = \frac{48k^2}{\pi^2}\int_0^\infty dr r^2 A(k,\xi(k;r)-\tilde{\omega})f(\xi(k;r)-\tilde{\omega}) \quad (3)$$

where the factor k^2 is from the spherical integration and $r=|\mathbf{r}|$ is the radial position in the trap. The prefactor here results by expressing wave vectors in units of k_F, energies in units of E_F, and radial positions in units of the Thomas-Fermi radius $R_F=[2E_F/(m\omega_0^2)]^{1/2}$ where $\omega_0=(\omega_x\omega_y\omega_z)^{1/3}$ is the average trap frequency.

Finally, to obtain an expression that can be directly compared with the experimental EDC spectra, it is sufficient to express the frequency $\tilde{\omega}$ in Eq. (3) in terms of the single-particle energy $E_s=k^2/(2m)-\tilde{\omega}$ via the relation $\xi(k;r)-\tilde{\omega}=E_s-\mu(r)$, where $\mu(r)=\mu-m\omega_0^2r^2/2$ is the local chemical potential in the harmonic trap. This yields eventually:

$$\mathrm{EDC}(k,E_s) = \frac{48k^2}{\pi^2}\int_0^\infty dr\, r^2 A(k,E_s-\mu(r))f(E_s-\mu(r)). \quad (4)$$

The numerical results obtained from Eq.(4) are then convoluted by a Gaussian broadening with a rms of about $0.25E_F$, corresponding to the experimental resolution.

When the interparticle interaction is switched off, $A(k,E_s-\mu(r);r)$ is given by $\delta(E_s-k^2/(2m))$. This defines the *zero* of the single-particle energy in the EDC curves as the energy of an isolated atom at rest. The chemical potential has thus disappeared from the free-particle branch $k^2/(2m)$, which remains positive for all k and can be used to reckon the value of the pseudogap.

Experimental procedures

We refer to Ref. [5] for a detailed description of the experimental techniques and procedures. Here, we add a few comments that are specifically relevant to the data presented in the main paper.

These data are taken at $T/T_c = 1.0\pm0.1$, where T_c is determined in the trapped system by the vanishing of the measured condensate fraction. Note, however, that, because the density of the trapped gas is spatially inhomogeneous, the local critical temperature decreases away from the cloud center.

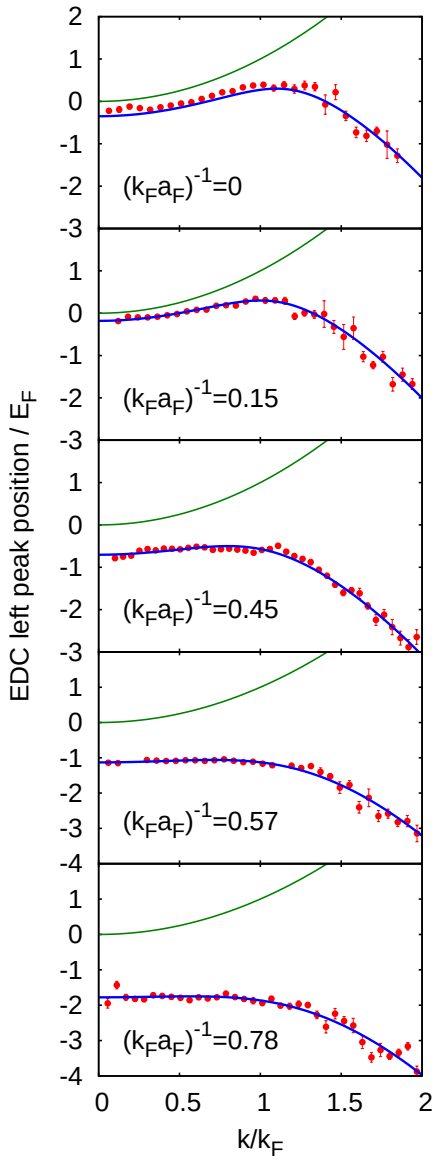

FIG. S1. χ^2-fit to the experimental data. The experimental data of Fig. 2(a) of the main paper (circles) are fitted over the interval $0.0 \leq k/k_F \leq 2.0$ by the BCS-like dispersion of Eq.(5) (full lines). The free-particle dispersion $k^2/(2m)$ is also shown for comparison (thin full lines).

It was already remarked in the main paper that an *absolute* comparison can be made between the experimental and theoretical EDC curves at given coupling and wave vector, in such a way that only their overall integral over k and E_s (and not the individual EDC curves) are normalized to unity. This is possible because the experimental radio frequency data (from which the EDC curves are obtained) were taken for the first time over a wide range of $\tilde{\omega}$, such that their long high-frequency tail could be determined and accurately compared with the $\tilde{\omega}^{-3/2}$ behavior predicted theoretically [2].

The experimental data reported in Fig. 2(a) of the main paper have been analyzed in terms of the BCS-like dispersion:

$$E_s(k) = \tilde{\mu} - \sqrt{\left(\frac{k^2}{2m} - \frac{k_L^2}{2m}\right)^2 + \tilde{\Delta}^2} \qquad (5)$$

where $k_L \approx k_F$ is the special wave vector about which the back-bending occurs and $\tilde{\mu}$ accounts for an overall (upward) displacement of the dispersion curves. Note that, contrary to the homogeneous case, in a trap $\tilde{\mu}$ is *not* related to the value of the thermodynamic chemical potential close to T_c.

A χ^2-analysis of the data in the interval $0.0 \leq k/k_F \leq 2.0$ yields the fits shown in Fig. S1. The five values of k_L thus obtained have been reported (together with the corresponding error bars) in Fig. 3(b) of the main paper (there, the additional value for the coupling $(k_F a_F)^{-1} = 1.1$ has been inferred from the experimental data reported in Ref.[4]).

The same analysis also shows that pairs of $(\tilde{\mu}, \tilde{\Delta})$ with $\tilde{\mu} - \tilde{\Delta} =$ constant produce comparable χ^2 tests. From Eq.(5) we note that $\tilde{\mu} - \tilde{\Delta} = E_s(k_L) \equiv E_{\max}$ corresponds to the maximum value of $E_s(k)$. For the five couplings here considered we obtain the values $E_{\max}/E_F = (0.40, 0.24, -0.5, -1.1, -1.8)$, in the order.

Using these values, one can extract a rough estimate of a (trap averaged) pseudogap energy, by relating them with the free-particle dispersion $k^2/(2m)$ at k_L. The k^2-dispersion can, in fact, be considered as *a lower bound* to the dispersion of the upper branch in the EDC curves, which results from the two-peak structure of $A(k,\omega)$ in the presence of a pseudogap [1] and behaves like $k^2/(2m)$ for $k_F \ll k$. [In the analysis of the experimental data the visibility of this upper branch is suppressed by the presence of the Fermi function.] The values we obtain for $[k_L^2/(2m) - E_{\max}]/2$ are $(0.38, 0.34, 0.58, 0.82, 1.08)E_F$ for the five couplings of Fig. S1, which are in line with the expected trend for the pseudogap of a homogeneous system (cf. Fig. 17 of Ref.[1]).

Determination of k_L for a homogeneous system

A comment is in order about the procedure for identifying the Luttinger wave vector k_L for a homogeneous system, as reported in Fig. 3(a) of the main paper.

Quite generally, $A(\mathbf{k},\omega)$ given by Eq.(1) has a pronounced peak when the following condition is satisfied

$$\omega - \xi_{\mathbf{k}} - \mathrm{Re}\Sigma(\mathbf{k},\omega) = 0 \qquad (6)$$

and provided $\mathrm{Im}\Sigma(\mathbf{k},\omega)$ is sufficiently small. In a BCS-like situation we write:

$$\Sigma(\mathbf{k},\omega) \approx \frac{\Delta_{\mathrm{pg}}^2}{\omega + i\eta + \xi_{\mathbf{k}} + \delta\mu} + \delta\mu \qquad (7)$$

with $\eta = 0^+$ and $\delta\mu = \mu - \mu_L$ where $\mu_L = k_L^2/(2m)$. Note that the shift $\delta\mu$ is the part of the self-energy which is

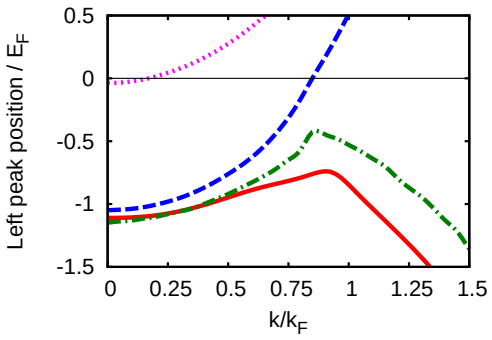

FIG. S2. Evolution in temperature of the dispersion $\omega(k)$ obtained by following the peak at lower energy in $A(k,\omega)$ for a homogeneous system at unitarity. The four curves correspond to temperatures $T/T_c = (1.0, 1.2, 1.65, 4.0)$ from bottom to top.

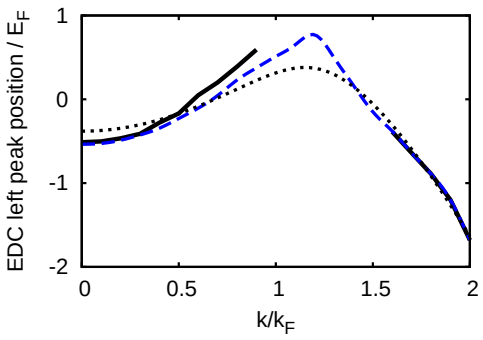

FIG. S3. The dispersion (two arcs drawn by full lines) of the low-frequency peak of $A(k,\omega)$ for a homogeneous system with the density of the shell at $r = r_{\max}$ for the coupling $(k_F a_F)^{-1} = 0.15$, is compared with the corresponding dispersion (dashed line) obtained multiplying $A(k,\omega)$ by $f(\omega)$. A BCS-like fit to the two arcs is also shown (dotted line).

responsible for the persistence of a remnant Fermi surface about the (temperature dependent) Fermi wave vector of the underlying non-interacting system. A combination of Eqs.(6) and (7) then yields:

$$\omega \approx -\sqrt{(\xi_{\mathbf{k}} + \delta\mu)^2 + \Delta_{\rm pg}^2} = -\sqrt{\left(\frac{k^2}{2m} - \frac{k_L^2}{2m}\right)^2 + \Delta_{\rm pg}^2} \tag{8}$$

for the lower branch (which has the largest spectral weight for $k \lesssim k_L$), where ω is measured with respect to the chemical potential. The maximum value $\omega \approx -\Delta_{\rm pg}$ is for $k = k_L$ where the back-bending occurs. For increasing temperature such that $\Delta_{\rm pg}$ closes up eventually, Eq.(6) yields accordingly $k = k_L$ for $\omega = 0$, which corresponds to the familiar condition for a Fermi liquid [6].

Figure S2 shows a typical temperature evolution of the dispersion $\omega(\mathbf{k})$ obtained by following the peak at lower energy in $A(\mathbf{k},\omega)$, from which the value of $k = k_L$ is extracted according to the above criterion. At sufficiently high temperatures when the dispersion $\omega(\mathbf{k})$ crosses zero, k_L is seen to quickly converge to the value associated with the temperature dependent chemical potential of the non-interacting Fermi system.

Additional theoretical analysis of the experimental data

In the expression (4) the presence of the Fermi function $f(\omega)$ may be of considerable help for the analysis of the dispersion of the low-ω peak, in situations when two broad non-Lorentzian structures in $A(k,\omega)$ merge together over a limited range of k. This is because multiplication of $A(k,\omega)$ by $f(\omega)$ in that expression acts effectively as a "filter" for the low-ω structures of $A(k,\omega)$, in particular for those values of ω through which the back-bending occurs in the dispersion.

This is shown explicitly in Fig. S3, where the dispersion of the low-ω peak of $A(k,\omega)$ (corresponding to a homogeneous system with the density of the shell at $r_{\max}$ for the trap coupling $(k_F a_F)^{-1} = 0.15$) is drawn (full line) only for those values of k for which two peaks in $A(k,\omega)$ appear clearly distinguishable. This procedure results in two arcs separated by an empty window. A single BCS-like fit (dotted line) to these two disconnected arcs via Eq.(5) provides the value $\tilde{\Delta}(r_{\max})/E_F = 0.77$, in reasonable agreement with the value determined for the whole trap. Figure S3 shows also the dispersion (dashed line) obtained by multiplying $A(k,\omega)$ by $f(\omega)$, in such a way that the low-ω peak can be smoothly followed even in the k-window that had to be excluded before. This procedure does not appreciably alter the values obtained by the BCS-like fit.

This conclusion is consistent with the fact that the lack of a spectral depression in $A(k,\omega)$ in a *limited* range of k does not necessarily lead to disappearance of the pseudogap in integrated quantities, like the single-particle density of states (DOS) [8], where a spectral depression survives at much higher temperature than in $A(k \approx k_F, \omega)$ [cf. the inset of Fig.4(b) of the main paper, where a calculation of the DOS is explicitly reported].

The presence of the factor $f(\omega)$ in Eq.(4) obviously affects more the large-ω than the low-ω peak of the EDC curves. The discrepancies that are evident in the large-ω peak from Fig. 1 of the main paper, when comparing experimental and theoretical EDC curves at T_c for the couplings 0.45 and 0.57, can accordingly be attributed to the larger absolute values of T_c at which the theoretical spectra are calculated [7], with respect to the experimental values of T_c at which the data are taken.

In Fig. S4 we reproduce the experimental EDC (circles) from Fig. 1 of the main paper for the two couplings 0.45

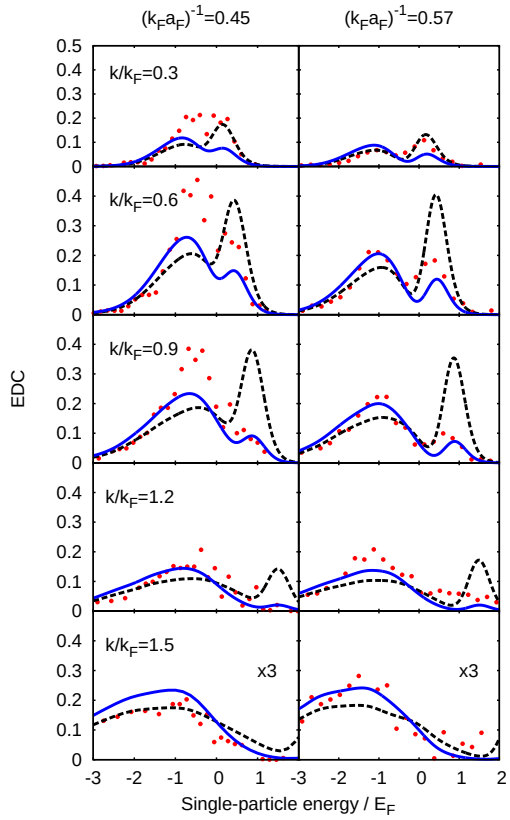

FIG. S4. The experimental EDC (circles) for the two couplings 0.45 and 0.57 are reproduced from Fig. 1 of the main paper, and compared with theoretical calculations (full lines) in which the temperature in the Fermi function has been decreased to $0.7T_c$. The theoretical curves reported in Fig. 1 of the main paper are also reproduced here (dashed lines).

and 0.57, and compare them with the theoretical calculations (full lines) in which the temperature in the Fermi function has been decreased to $0.7T_c$ while the temperature in $A(k,\omega)$ is kept at T_c. This procedure is consistent with the fact that in this coupling range the theoretical approach overestimates the absolute value of T_c by about 30%, while close to T_c the spectral function depends essentially on the relative temperature T/T_c. This procedure, albeit empirical, goes in the right direction of reducing the height of the high-ω peak of the EDC curves making it closer to the experimental value, while affecting only slightly the low-ω part of the EDC curves.

The numerical difference between the theoretical and experimental values of T_c for a homogeneous Fermi gas at unitarity is also evident from Fig. 4(c) of the main paper, although this difference is immaterial to the sake of the argument that was there raised.

Specific heat of a non-interacting Fermi gas

In Fig. 4(c) of the main paper the behavior of the specific heat of a non-interacting Fermi gas was reported for

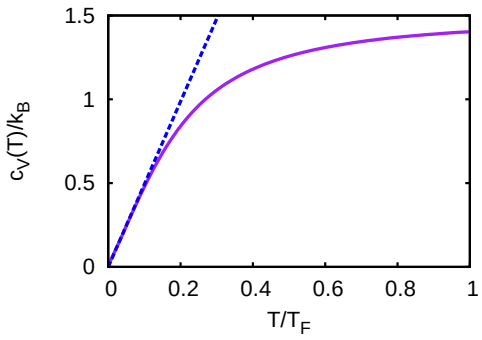

FIG. S5. Specific heat per particle of a non-interacting Fermi gas (full line) reported over an extended temperature range. The dashed line corresponds to the linear behavior that holds when $T/T_F \ll 1$.

comparison over the temperature interval $0.2 \lesssim T/T_F \lesssim 0.6$, which was relevant to the experimental data shown in the same figure.

It is interesting to show the same quantity over a more extended temperature range which reaches $T = 0$. This is done for $0 \leq T/T_F \leq 1$ in Fig. S5, where the specific heat per particle of a non-interacting Fermi gas is reported vs T/T_F (full line) and compared with its *linear* approximation $(k_B\pi^2/2)\,T/T_F$ (dashed line) that holds when $T/T_F \ll 1$. Note that for $T/T_F = 0.2$ this linear approximation deviates from the full calculation already by about 20%.

An analogous linear behavior is known to result for a Fermi liquid when $T/T_F \ll 1$, although with a different slope reflecting the renormalization of the mass [9].

[1] A. Perali, P. Pieri, G. C. Strinati, and C. Castellani, Phys. Rev. B **66**, 024510 (2002).

[2] A. Perali, P. Pieri, and G. C. Strinati, Phys. Rev. Lett. **100**, 010402 (2008).

[3] P. Pieri, A. Perali, and G. C. Strinati, Nature Phys. **5**, 736 (2009).

[4] J. T. Stewart, J. P. Gaebler, and D. S. Jin, Nature **454**, 744 (2008).

[5] J. P. Gaebler, J. T. Stewart, T. E. Drake, D. S. Jin, A. Perali, P. Pieri, and G. C. Strinati, Nature Phys. **6**, 569 (2010).

[6] E. M. Lifshitz and L. P. Pitaevskii, *Statistical Physics: Theory of the Condensed State* (Butterworth-Heinemann, Oxford, 1980), Section 14.

[7] A. Perali, P. Pieri, L. Pisani, and G. C. Strinati, Phys. Rev. Lett. **92**, 220404 (2004).

[8] S. Tsuchiya, R. Watanabe, and Y. Ohashi, Phys. Rev. A **80**, 033613 (2009).

[9] See, e.g., D. Pines and P. Nozières, *The Theory of Quantum Liquids: Normal Fermi Liquids* (Addison-Wesley, Reading, 1996), Section 1.3.